TESTING AND ANALYSIS OF GRID-STIFFENED COMPOSITE STRUCTURAL PANELS

S. Giannis[a, *], A. Hajdaei[a], V. Matěják[a], A. Toulitsis[a]

[a] *Element Materials Technology Ltd, Wilbury Way, Hitchin, SG4 0TW, United Kingdom*
** stefanos.giannis@element.com*

Keywords: Grid-stiffened, Carbon, Fuselage, FE Analysis

Abstract
A composite fuselage structure has been developed in WASIS project based on the lattice stiffening concept, thus optimizing geometrical and mass characteristics of transition zones of structural joints. To understand the mechanical performance and validate the design methodology of the proposed structure a testing programme following a building block approach and involving structural parts of different levels of complexity was devised and executed. In this paper the experimental results derived for grid-stiffened components representing different areas in the fuselage section are presented. These tests were then used to validate a numerical approach hence leading to a representative global model of the structure that can capture localised failures under realistic loading conditions.

1. Introduction

Composite materials are nowadays extensively used in aeronautics with Boeing's 787 Dreamliner and Airbus's XWB 350 being the leading examples in civil aviation. Nevertheless, the design of primary composite structures, such as fuselage, follows somewhat traditional methodologies with spars and ribs acting as the stiffening and load carrying media. An alternative approach would be to develop a composite fuselage structure based on the lattice stiffening concept, thus optimizing geometrical and mass characteristics of transition zones of fuselage structural joints. This was the main aim of the WASIS project.

A two metre long section of the Piaggio P180 aircraft was considered as the working platform and an integrated grid-stiffened composite structure was designed. Two manufacturing methods were investigated, Filament Winding (FW) and Automated Tape Placement (ATP). The proposed design methodology and the selection of the manufacturing approach were complemented with a test programme aiming to evaluate the performance and validate the design of the lattice grid-stiffened composite structure. A testing building block approach was devised following established procedures highlighted in CMH-17 for small business aircraft (see Figure 1) and was previously presented in [1]. Since laminae and laminate material properties alone are not sufficient for the prediction of the behaviour of the full-scale structure, multiple tests were performed on component level, investigating the performance of critical areas (i.e. rib intersections, attachment frame connections) of the structure. Component tests were used to determine the most critical failure modes and redesign the structure increasing the corresponding margins of safety.

Results of the experimental programme are presented in this paper, together with the approach used to benchmark the global finite element models.

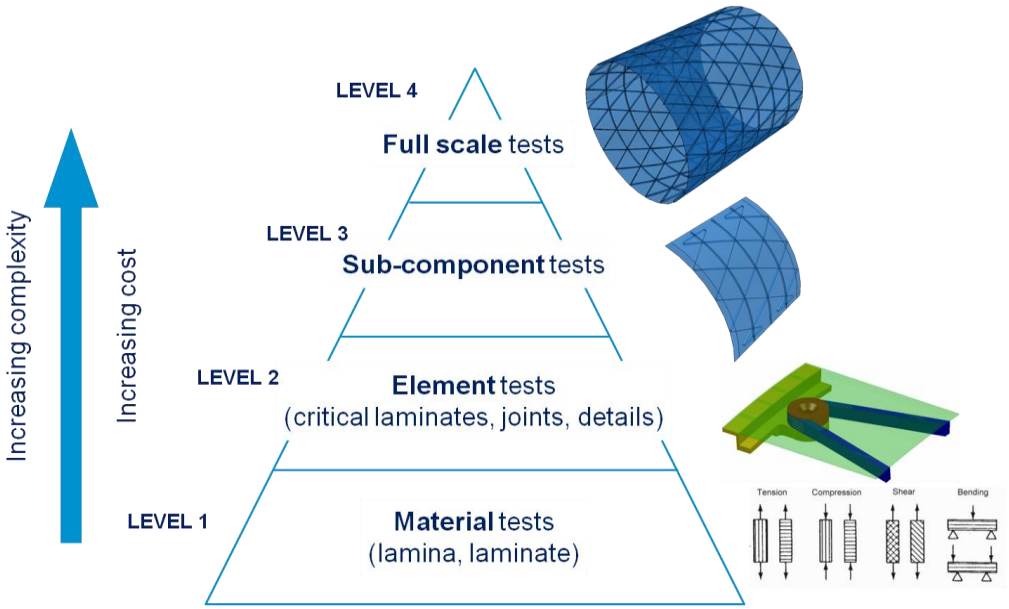

Figure 1. Building block approach for testing and validation of the grid-stiffened fuselage structure

2. Experimental Approach

Experiments on grid-stiffened parts of different levels of complexity were performed in order to investigate the performance and validate the design of the structure. These included three-rib intersections and attachment frame rib terminations. In addition, composite components with and without the presence of integrated skin laminate were considered. In all cases the ribs comprised unidirectional wet wound Tenax-E HTS40 (12K) carbon fibre reinforced Araldite LY556 epoxy, while the skin was formed in a ±45° configuration. All parts were cured for 2 hours at 80ºC, followed by a free standing post-cure cycle for 6 hours at 120°C. In the following paragraphs, the details of the experimental approach are presented.

2.1. Specimen preparation

For uniform application of the load on specimen's skin and stiffening ribs, the end part was potted in resin. The resin used was the RenCast CW 2418-1/HY 5162 metal filled epoxy system by Huntsman. The potted specimen ends were machined to remove the excess resin and reveal the composite end. This provided the required contact surface to transfer the compression load directly to the composite in addition to the one transferred via shear at contact surfaces of the composite and resin. Accurate machining also ensured two parallel surfaces for uniform application of the load on all sections of the composite specimen. A similar approach has also been presented in [2]. Photographs of the prepared specimens prior to testing are given in Figure 2 for specimens comprising three-ribs intersection with skin (Type 1), three-ribs intersection without skin (Type 2), attachment frame details with skin (Type 3) and attachment frame detail without skin (Type 4). The physical dimensions of Type 3 and Type 4 specimens were the same as the full scale 1.8 m diameter designed fuselage barrel, while those for Type 1 and Type 2 specimens were from a scaled down barrel (0.5 m in diameter).

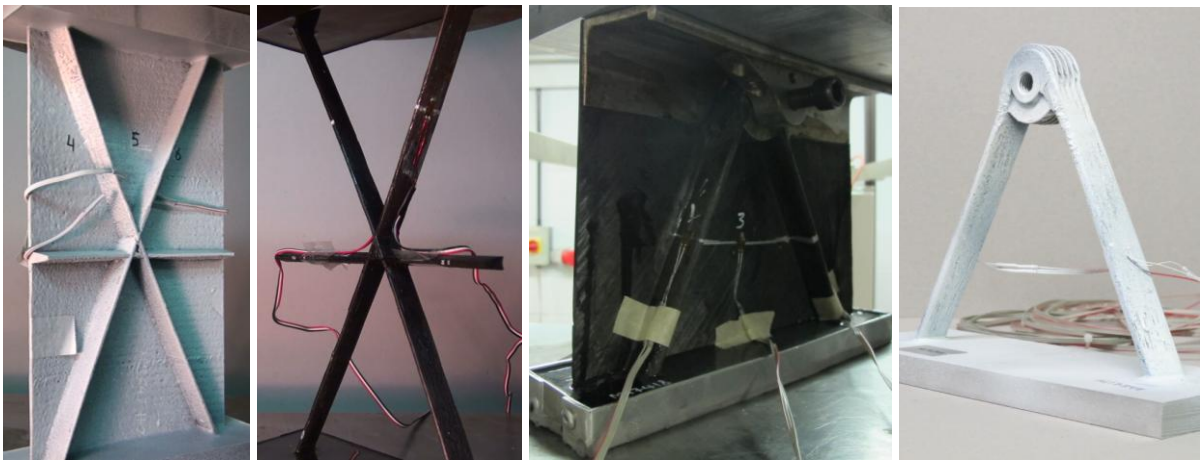

Figure 2. Geometry of the various types of critical components considered

2.2. Testing

All tests were contacted on a Zwick Z250 universal test machine, equipped with a 250kN load cell. The load was applied on the specimen via controlled crosshead movement at a rate of 0.25 mm/min. To measure the response of the grid-stiffened structural elements a number of strain gages were attached on various locations on each specimen. For those that only contained ribs (Type 2 and 4), strain gauges were bonded on each rib along its physical axis, which coincided with the load path. For the cases that structural parts with skin and ribs were tested, a number of strain gauges were also attached at locations on the skin, in order to monitor the uniformity of deformation of the structure as well as to detect local buckling phenomena.

3. Experimental Results

3.1. Type 1 and Type 2

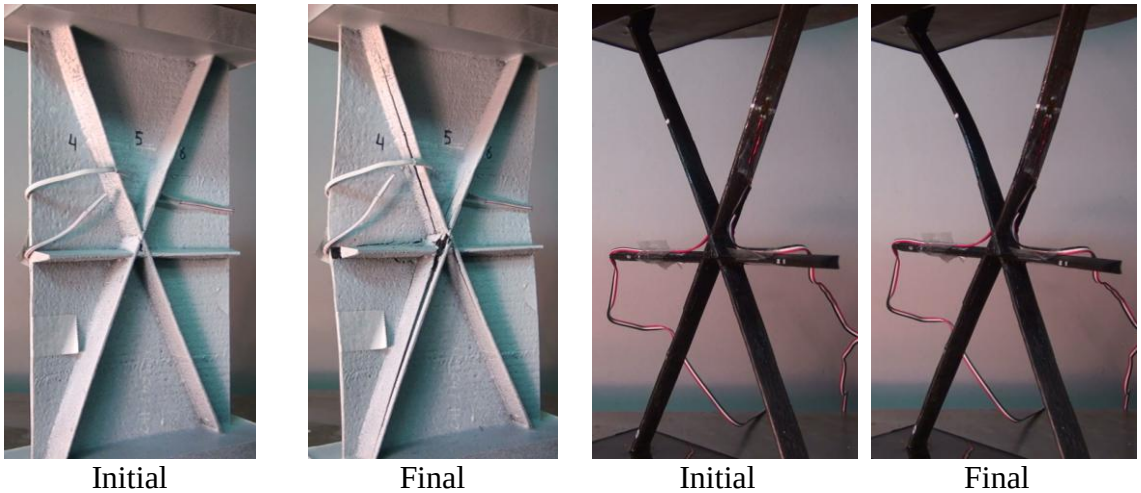

Figure 3. Deformation prior to loading and just after failure occurred for Type 1 and Type 2 components

The deformation of Type 1 and Type 2 components at the point of failure is illustrated in the photographs in Figure 3. For Type 1 components there was significant out-plane deformation

of the skin at the edges of the component as well as in the middle (upper triangular area) as demonstrated by the local strain measurements. The deviation from linearity found for all four strain gauges above 20 kN in Figure 4(b) is attributed solely to the local buckling of the skin. The ribs continue to carry load in a linear manner up to failure. The local buckling of the skin had a detrimental effect on the failure of the component. This can be described as a combination of skin-to-ribs debonding and local compressive failure of the ribs.

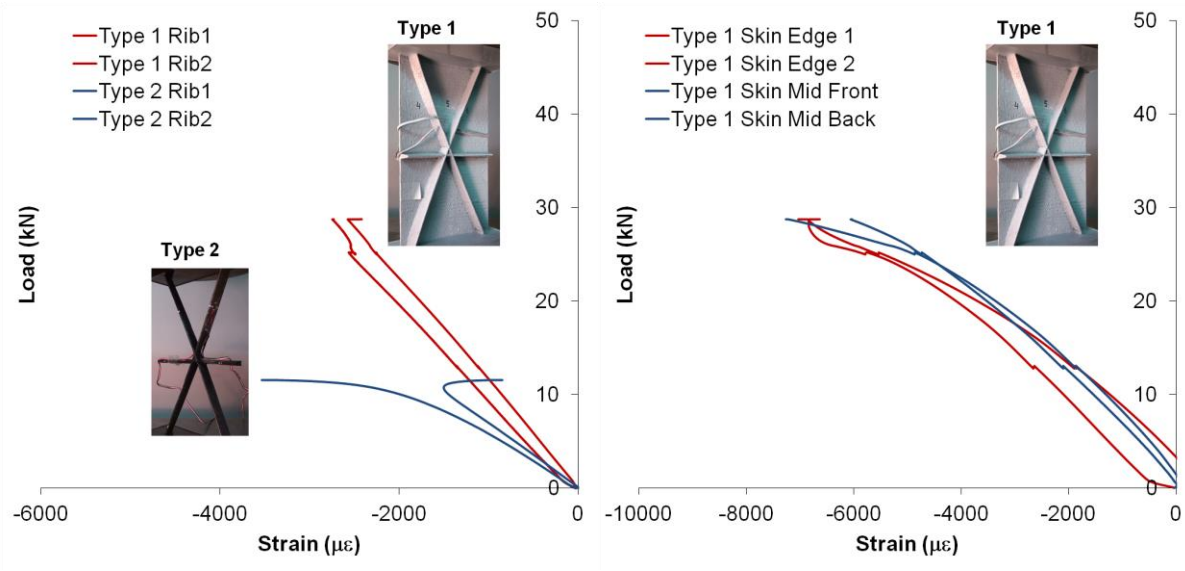

(a) (b)

Figure 4. Local strain measurements for (a) Type 1 and Type 2 components on the ribs and (b) Type 1 component on the skin

The behaviour of the Type 2 components was somehow different as the omission of the skin led to the instability of the ribs at a much lower load level. Deviation from linearity (see Figure 4(a)) occurred just after 10 kN and the ribs continue to deform substantially prior to failing locally in compression.

3.2. Type 3 and Type 4

The experimentally obtained results for Type 3 and Type 4 components are presented in Figure 5(a). The load to failure appears to be very similar for both types of components, however, the deformation and failure mechanics were found to be vastly different. Type 4 components didn't contain any skin and the loading was applied directly to the metallic reel through a pin. The load was then transferred to the ribs via shear of the adhesively bonded and mechanically interlocked area around the reel. Failure occurred at this area and as shown in the micrograph in Figure 5(b) there was debonding between the metallic reel and the composite. The existence of resin poor areas and dry fibres deep in the reel base indicates deviations in manufacturing and it is believed that have definitely compromised the failure load of the joint.

Regarding the Type 3 components, the load path was both through the metallic reel to the unidirectional ribs, and through the metallic attachment to the skin via shear. The failure of these components characterised by skin-to-ribs separation prior to failure around the metallic reel in a similar manner to the Type 4 components.

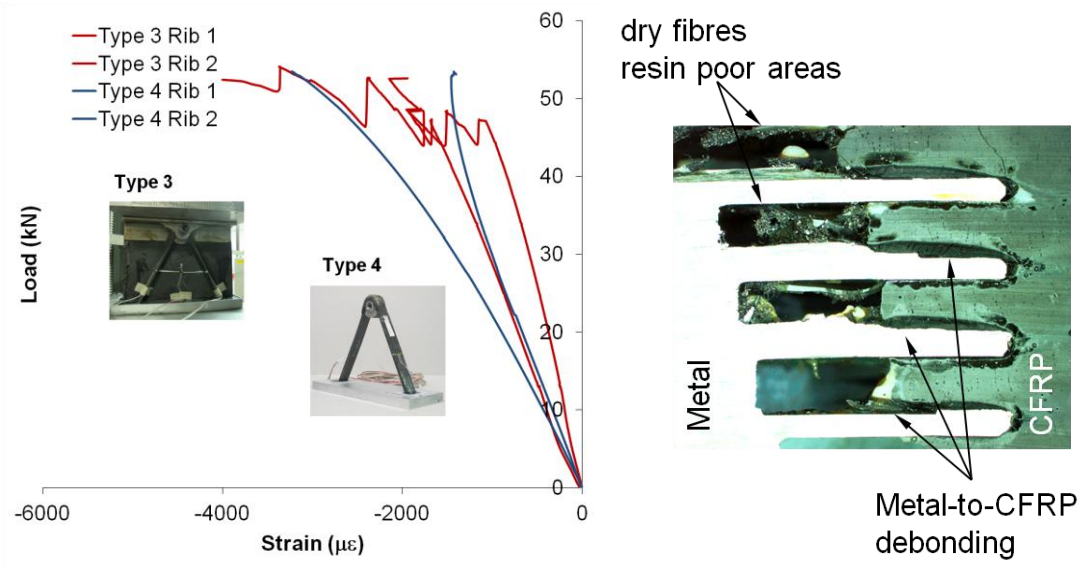

(a) (b)

Figure 5. (a) Local rib strain measurements for Type 3 and Type 4 components and (b) micrograph of failure in the metallic reel area

The measured macroscopic loads to failure and the locus of failure are presented in Table 1.

Specimen Type	Failure Load (kN)	Failure Type
1	29 - 33	Ribs compression / skin-to-rib debond
2	11- 12	Ribs buckling and ribs compression
3	54 - 62	Skin-to-ribs debond / reel failure
4	29 - 53	Reel failure

Table 1. Summary of the failure loads and failure type for the different types of components tested

Based on the experimental results it can be concluded that the skin carries a significant amount of load and prevents / delays buckling of ribs, however, the relatively high stiffness mismatch between the ±45° skin laminate and the unidirectional ribs leads to debonding and subsequent failure of the ribs in compression. This can be avoided by through thickness connections (i.e. Z-pinning) between the skin and the ribs. In addition, the reel can carry even up to 53 kN of load prior to debonding and failure, but further optimisation of the carbon fibres locally prior to curing can increase the contact area and lead to even higher load carrying capability.

4. Analysis

4.1. Geometrical models of components

Type 1 and Type 2 specimens were modelled in order to validate the numerical approach. The finite element model geometry was created as a cut-out of the fuselage scaled section (Figure 6), which was a cylinder with diameter of 500 mm and height of 250 mm. One hoop rib and 12 pairs of spiral ribs are connected to the inner diameter of a 1.6 mm thick skin. All ribs have trapezoidal profile with dimensions shown in Figure 6. The hoop rib is not intersecting the spiral ribs exactly at their intersection, but is slightly shifted from the central position due to manufacturing constraints. The free compression length of the parts is reduced by 20 mm from each side to account for the area that is potted in resin for uniform application of the compressive loads. This is achieved by applying fixed displacement boundary

conditions to the areas representing the potted portion. Both variations of the component (i.e. with and without skin) were modelled at first by 2D shell elements with Abaqus Hashin failure criteria and then as 3D elements with user failure criteria by means of user defined subroutine. For the 2D shell elements, Standard and Riks integration schemes were utilized during simulation, because compressive load on a thin walled structure causes unstable, geometrically nonlinear response and buckling, for which Riks method is better suited.

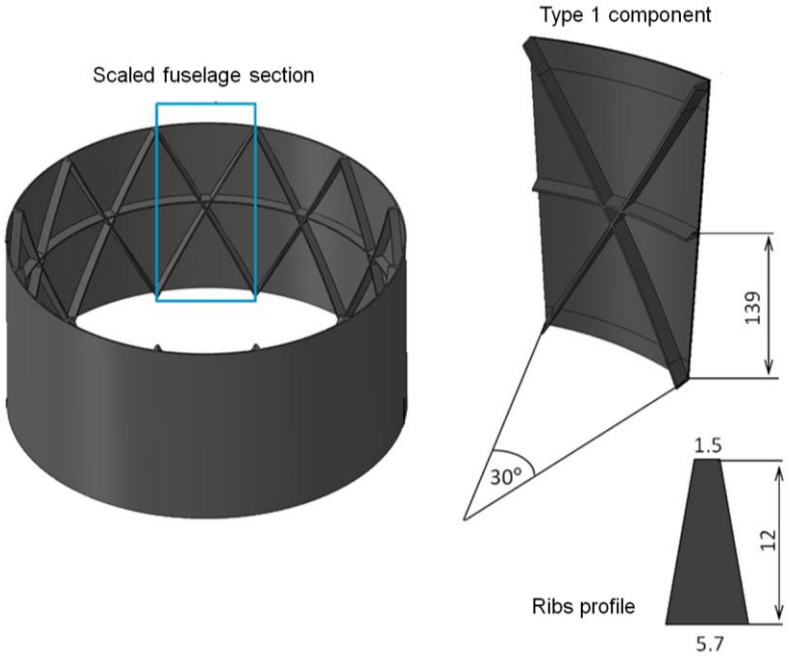

Figure 6. Model geometry for Type 1 component

4.2. Numerical validation results

The results of a total of seven finite element models are presented in Table 2. For Type 1 components, both shell and solid models predicted very well the experimental stiffness obtained from local strain measurements, as well as the local buckling of the skin as shown in Figure 7. It was also apparent that simplifying and modelling the ribs cross section as constant led to over estimation of the failure load. Overall the solid element models predicted much better the failure load and captured the local deformation more accurately. For Type 2 components, shell models also over predicted the experimentally obtained strength, although they captured the macroscopic deformation of the component (see Figure 7). The solid model predicted accurately the initial fibre failure, but it presented further deformation until complete failure associated with instability of the ribs.

Specimen Type	Model Name	Element Type	Ribs x-Section	Failure Load (kN)
1	V1Std-NA	shell	constant	45.3
	V2Std-NA	shell	constant	38.3
	V21Std-NA	shell	variable	35.8
	UMAT-NA	solid	-	33.2
2	V1Std-NA	shell	constant	21.7
	V11Std-NA	shell	variable	19.2
	UMAT-NA	solid	-	11.5

Table 2. Summary of the different numerical models and predicted failure loads

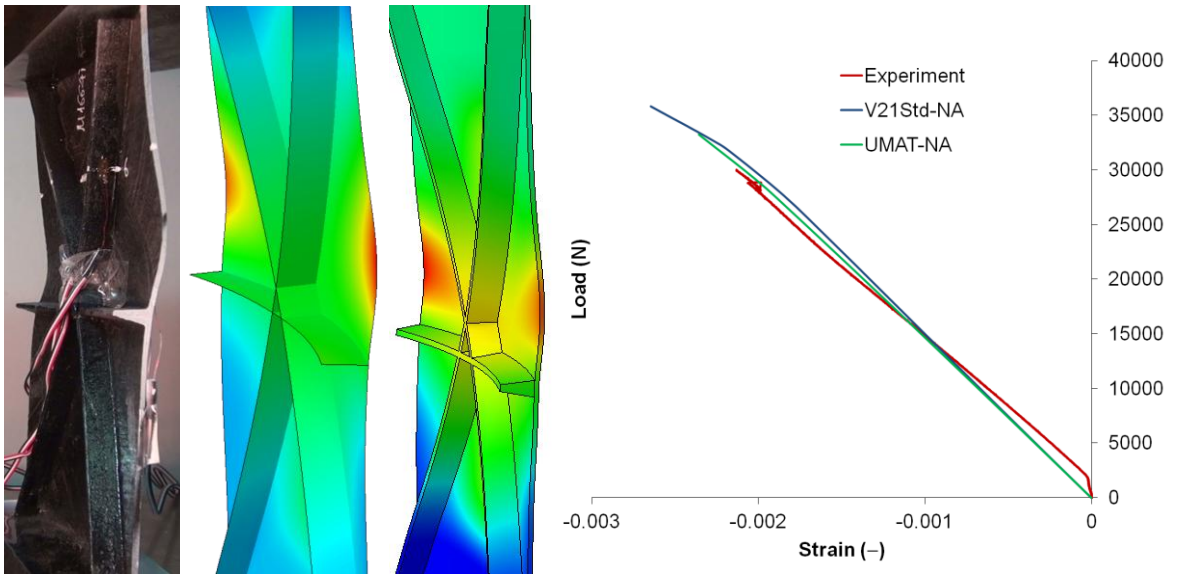

Figure 7. Comparison of modelling results and experimental deformation shape and local strains for Type 1 component

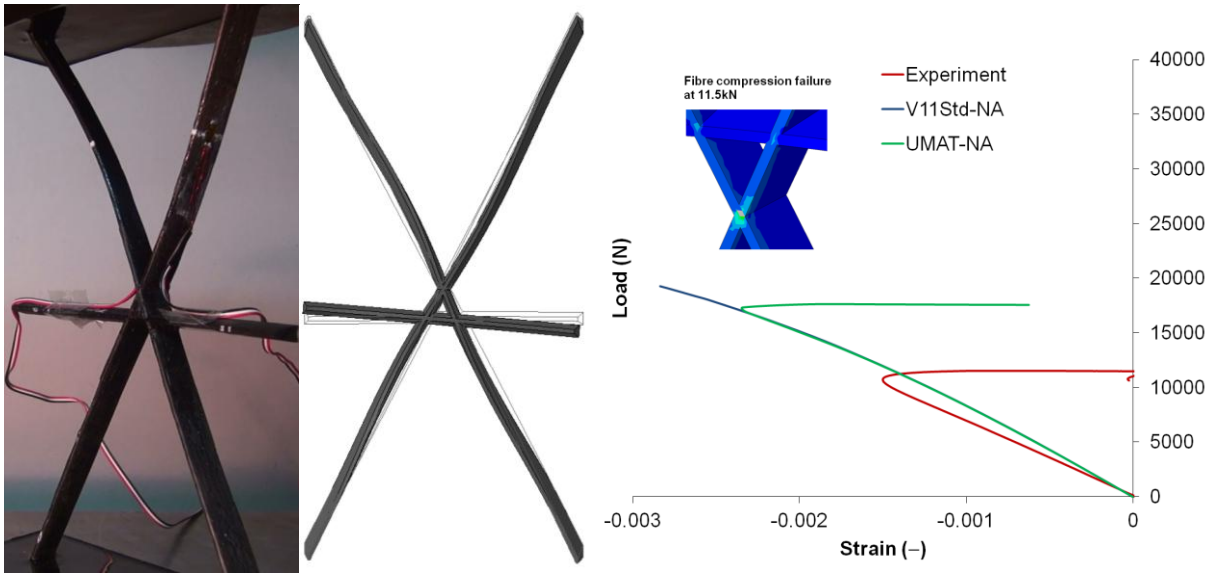

Figure 8. Comparison of modelling results and experimental deformation shape and local strains for Type 2 component

4.3. Global-local model

The global model can in principal be constructed using shell elements since these are very effective for modelling thin walled structures and composite laminates in particular. First ply failure criteria can be used on global scale to evaluate load carrying capacity and overall response of the global model. However, there are some issues and limitations when using a shell-to-solid sub-modelling approach and therefore solid representation of the global model is necessary to obtain correct driving boundary conditions for a detailed solid sub-model. The successful simulation of the Type 1 and Type 2 components using solid elements also meant that the local sub-models need to be represented with solid elements. A parametric geometry generation algorithm was created in Python and loading was applied in three different directions, along the length of the two metre fuselage (Figure 9). Tail down landing at maximum landing weight was selected as the critical load case for the analysis.

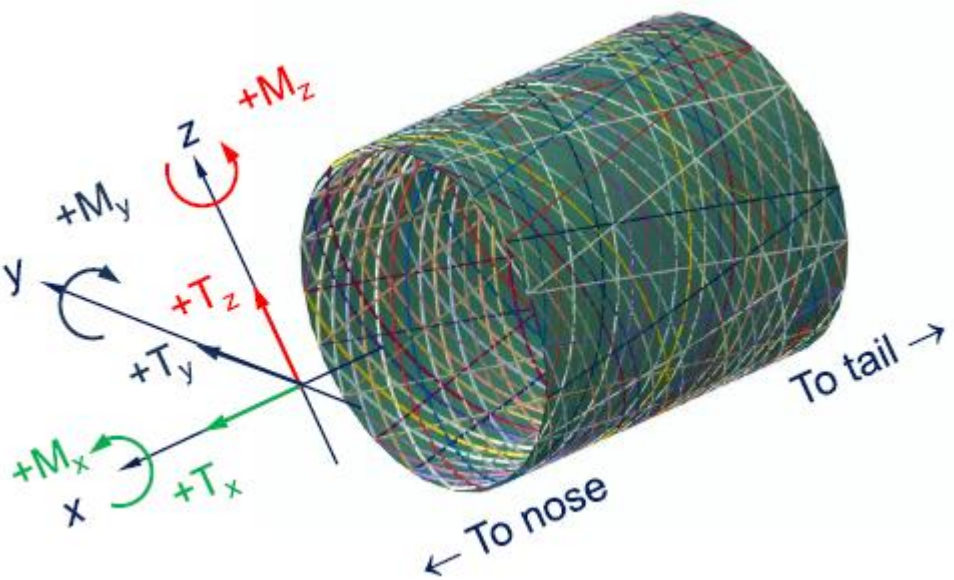

Figure 9. Fuselage section and notation of applied loading

Under the applied loading conditions the failure modes of delamination between the skin and the ribs and the matrix failure in tension were found (see Figure 10). The maximum stress failure criterion indicated failures close to the ribs cross sections associated both with matrix tension and a fibre compression.

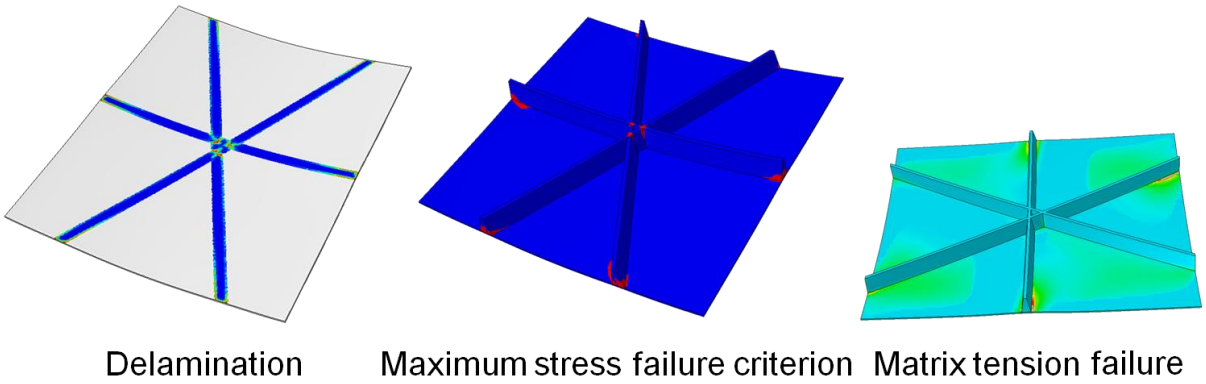

Figure 10. Fuselage section and notation of applied loading

5. Conclusions

An experimental programme following a building block approach has been implemented and the failure of grid-stiffened parts was quantified and understood. The experimental results were then used to successfully validate a modelling approach in order to increase confidence in a global-local numerical study and predicted failures in the structure due to the application of a realistic complex loading scenario.

References

[1] S. Giannis, S. Frenz and B. Araujo. A Building Block Approach for Testing and Evaluating the Performance of an Integrated Lattice Fuselage Section. In *17th International Conference on Composite Structures*, 2013.

[2] A. C. Biskner, J. E. Higgins. Testing and Analysis of large Curved Grid-Stiffened Composite Panels. In *16th International Conference on Composite Materials*, 2007.